Structural Distortions of the Metal Dichalcogenide Units in AMo_2S_4 ($A = V$, Cr, Fe, Co) and Magnetic and Electrical Properties

Paz Vaqueiro, M. Laura Kosidowski, and Anthony V. Powell*

Department of Chemistry, Heriot-Watt University, Edinburgh EH14 4AS, United Kingdom

Received August 7, 2001. Revised Manuscript Received January 2, 2002

Powder neutron diffraction data collected for AMo_2S_4 ($A = V$, Cr, Fe, Co) reveal that the materials crystallize in the space group *Cc* ($a \approx 11.8$ Å, $b \approx 6.5$ Å, $c \approx 13$ Å, $\beta \approx 114°$). The structure consists of dichalcogenide (MS_2) layers of edge-sharing octahedra, separated by a layer in which 50% of cation sites are occupied in an ordered fashion. Cations in the MS_2 unit are distorted from an ideal hexagonal array. For the early transition series cations A = Cr, V, the distortion involves the formation of triangular clusters of cations, whereas for A = Fe, Co diamond-shape cation clusters are observed. The semiconducting properties of these materials are discussed in light of these results. Both $FeMo_2S_4$ and $CoMo_2S_4$ order antiferromagnetically with $T_N = 110$ and <300 K, respectively. Low-temperature powder neutron diffraction data demonstrate that both materials have a similar magnetic structure and that the ordered magnetic moments ($\mu(Fe) = 3.16(3)\mu_B$, $\mu(Co) = 2.14(3)\mu_B$) are confined to the A cations in the vacancy layer.

Introduction

Many transition metal sulfides of stoichiometry M_3S_4 adopt the monoclinic Cr_3S_4 structure, which can be derived from a cation-deficient NiAs-type structure. In the NiAs structure, the cations (M) occupy octahedral sites between pairs of hexagonally close-packed anion (X) layers, resulting in the stacking sequence XMXMXMX. The introduction, in an ordered manner, of cation vacancies to alternate layers along the *c*-axis of the NiAs unit cell gives rise to a range of vacancy-ordered phases of general formula M_xMS_2 ($0 < x < 1$). In the Cr_3S_4 structure ($x = {}^1/_2$),[1] fully occupied layers alternate with half-occupied layers, corresponding to the stacking sequence $XMXM_{0.5}XMX$. This results in two crystallographically distinct cation sites, as indicated by the formulation $(M)[M_2]S_4$, where (M) and [M] denote sites in the vacancy and the fully occupied layers, respectively. For ternary phases AM_2S_4, two extreme cation distributions are possible. These correspond to the normal, $(A)[M_2]S_4$, and inverse, $(M)[AM]S_4$, structure types. Cation partitioning is, however, seldom complete,[2−4] and recent studies,[5−7] of ternary phases containing first-row transition metals, have shown that the distribution is dependent on the electronic properties of the constituent cations. In particular, cations drawn from the early part of the transition series show a greater preference for sites in the fully occupied layer. This may be related to the ability of such cations to delocalize electron density by direct $t_{2g}-t_{2g}$ interactions. Depending on the identity of the cations present in the fully occupied layer, distortions of the dichalcogenide slab may occur, to which the electrical transport properties are particularly sensitive.[8] For example, we have recently demonstrated[9] that the onset of metallization which occurs at a critical composition of $x_c \approx 0.6$ in $NiCr_{2-x}V_xS_4$ is associated with a structural distortion that results in the formation of zigzag chains of cations.

In seeking to extend our investigations of the relationship between the nature of the cation distortion and electrical transport properties, our interest has turned to materials containing the heavier congeners of chromium. Ternary molybdenum sulfides with the general formula AMo_2S_4 ($A = V$, Cr, Fe, Co) have been reported in the literature as being isostructural with Cr_3S_4 (space group *C*2/*m*).[10,11] In this space group, symmetry permits only distortions involving the formation of zigzag cation chains. However, other workers have suggested a lower symmetry space group (*Cc*) for $CoMo_2S_4$ and $FeMo_2S_4$[12] and a distortion which produces diamond-shape metal clusters in the fully occupied layer. Canadell et al.[8] have shown that there is a relationship between the nature of the distortion and the electrical transport properties of materials containing MS_2 units. Therefore, in an

---

* To whom correspondence should be addressed. Fax: +44 (0)131 451 3180. E-mail: a.v.powell@hw.ac.uk.

(1) Jellinek, F. *Acta Crystallogr.* **1957**, *10*, 620.
(2) Hayashi, A.; Ueda, Y.; Kosuge, K.; Murata, H.; Asano, H.; Wanatabe, N.; Izumi, F. *J. Solid State Chem.* **1987**, *71*, 237.
(3) Ueda, Y.; Kosuge, K.; Urabayashi, M.; Hayashi, A.; Kachi, S. *J. Solid State Chem.* **1985**, *56*, 263.
(4) Powell, A. V.; Ritter, C.; Vaqueiro, P. *J. Solid State Chem.* **1999**, *144*, 372.
(5) Powell, A. V.; Colgan, D. C.; Vaqueiro, P. *J. Mater. Chem.* **1999**, *9*, 485.
(6) Colgan, D. C.; Powell, A. V. *J. Mater. Chem.* **1997**, *7*, 2433.
(7) Colgan, D. C.; Powell, A. V. *J. Mater. Chem.* **1996**, *6*, 1579.
(8) Canadell, E.; LeBeuze A.; Abdelaziz El Khalifa, M.; Chevrel, R.; Whangbo, M. H. *J. Am. Chem. Soc.* **1989**, *111*, 3778.
(9) Vaqueiro, P.; Powell, A. V.; Bold, M.; Ritter, C. *Chem. Mater.* **2000**, *12*, 1034.
(10) van den Berg, J. M. *Inorg. Chim. Acta* **1968**, *10*, 216.
(11) Wada, H.; Onoda, M.; Nozaki, H.; Kawada, I. *J. Solid State Chem.* **1986**, *63*, 369.
(12) Guillevic, J.; Le Marrouille, J.-Y.; Grandjean, D. *Acta Crystallogr.* **1974**, *B30*, 111.

10.1021/cm010720k CCC: \$22.00

Table 1. Results of Thermogravimetry and Atomic Absorption Analysis

nominal composition	nominal Mo content (%)	experimental Mo content (%)	expected TGA weight loss (%)	experimental TGA weight loss (%)	experimental composition[a]
VMo_2S_4	51.7	49.1	79.8	78.4	$V_{1.08}Mo_{1.92}S_{4.2}$
$CrMo_2S_4$	51.9	51.6	79.6	79.1	$Cr_{1.01}Mo_{1.99}S_{3.9}$
$FeMo_2S_4$	50.6	51.0	78.8	78.3	$Fe_{1.04}Mo_{1.96}S_{3.9}$
$CoMo_2S_{3.93}$	52.6	50.9	41.9	42.8	$Co_{0.91}Mo_{2.09}S_{4.0}$

[a] Normalized to a total metal content of 3.

effort to resolve ambiguities over the symmetry of these phases and to establish the cation distribution, we have carried out a detailed structural study using powder neutron diffraction. The results of this investigation for AMo_2S_4 (A = V, Cr, Fe, Co) are presented here, together with a study of the transport and magnetic properties.

Experimental Section

All materials were synthesized by heating a stoichiometric mixture of the elements in evacuated silica tubes ($<10^{-4}$ Torr) at 1150 °C for periods of up to 5 days with intermediate regrinding. After the second firing, samples were cooled at 4 °C/min to 300 °C prior to removal from the furnace. The material $CoMo_2S_4$ was prepared with a slight deficiency in sulfur, corresponding to the stoichiometry $CoMo_2S_{3.93}$, to avoid the formation of MoS_2, as reported by Chevrel et al.[13]

The progress of the reaction was followed by powder X-ray diffraction, using a Philips PA2000 diffractometer with nickel-filtered Cu Kα radiation. The molybdenum content of the samples was determined by atomic absorption spectroscopy with an Instrumental Laboratories SII atomic absorption spectrometer. The sulfur content was determined thermogravimetrically by oxidation in a flow of dry oxygen on a Du Pont Instruments 951 thermogravimetric analyzer. The vanadium, chromium, iron, and cobalt contents were obtained by difference.

Time-of-flight powder neutron diffraction data were collected at room temperature on the Polaris diffractometer at ISIS, Rutherford Appleton Laboratory. For the materials containing iron and cobalt, data collection was also carried out at 4 K. In each case, data were collected on ca. 3 g of sample contained in thin-walled vanadium cans. Initial data manipulation and reduction was carried out using Genie[14] spectrum manipulation software. Neutron diffraction data, from the highest resolution backscattering bank of detectors ($2\theta = 145°$) and from the low-angle bank of detectors ($2\theta = 35°$), were summed and normalized for subsequent use in Rietveld refinements using the GSAS package.[15]

The electrical resistance of the samples as a function of temperature was measured using the four-probe DC technique. An ingot (~6 × 3 × 1 mm) was cut from a sintered pellet, four 50-μm silver wires were attached using colloidal silver paint, and connections were made to a HP34401A multimeter. The sample was mounted in an Oxford Instruments CF1200 cryostat connected to an ITC502 temperature controller. Measurements were carried out over the temperature range $77 \leq T/\mathrm{K} \leq 300$. Magnetic measurements were performed using a Quantum Design MPMS2 SQUID susceptometer. Samples were loaded into gelatin capsules at room temperature and data were collected over the temperature range $5 \leq T/\mathrm{K} \leq 320$, both after cooling in zero applied field (zfc) and in the measuring field (fc) of 1000 G. Data were corrected for the diamagnetism of the gelatin capsule.

Results

Powder X-ray diffraction data are consistent with the formation of single-phase materials, although subsequent examination of powder neutron diffraction data indicated the presence of trace amounts of Mo_2S_3 in the sample of VMo_2S_4. The results of the chemical analysis presented in Table 1 indicate generally good agreement between nominal compositions and those determined analytically. The slightly high sulfur content obtained for VMo_2S_4 reflects the fact that this sample contains small amounts of a Mo_2S_3 impurity. Diffraction data can be indexed on the basis of monoclinic unit cells, similar to both of the alternatives previously reported for the AMo_2S_4 phases. However, on the basis of the powder X-ray diffraction data alone, it was not possible to distinguish between the alternative space groups *Cc* and *C*2/*m*. Simulations confirm that both structures produce almost identical powder X-ray diffraction patterns.

Room-Temperature Powder Neutron Diffraction Data. Rietveld refinements using neutron diffraction data from the backscattering bank of detectors were carried out in the space groups *C*2/*m* and *Cc*. The lattice parameters of the *Cc* unit cell are related to those of the *C*2/*m* unit cell through the following matrix:

$$\begin{pmatrix} 0 & 0 & 2 \\ 0 & 2 & 0 \\ \bar{1} & 0 & \bar{2} \end{pmatrix}$$

Given the analytical data of Table 1, all structural models used nominal compositions. For VMo_2S_4, room temperature X-ray diffraction and neutron diffraction data were used simultaneously to establish the cation distribution between sites in the vacancy and fully occupied layers. In the initial structural models, A cations occupied vacancy layer sites, while Mo cations reside exclusively in the fully occupied layer. Background terms, peak shape parameters, lattice parameters, an overall thermal parameter, and atomic parameters were refined. For the material VMo_2S_4, regions centered at $d \approx 2.1$ Å and $d \approx 2.2$ Å were excluded from the neutron data, owing to the presence of the reflections $(11\bar{3})$ and (112) of Mo_2S_3 ($d_{11\bar{3}} = 2.102$ Å, $d_{112} = 2.243$ Å).[16] In both space groups, refinements using data for VMo_2S_4 resulted in miscalculations of peak intensities, and therefore cation site occupancy factors were introduced as variables into these refinements, with the constraint that the overall stoichiometry is maintained. For all AMo_2S_4 phases, refinements carried out in the space group *Cc* resulted in a better agreement between observed and calculated data, reflected in lower goodness-of-fit parameters ($\chi^2 = 2.0-4.3$, $R_{wp} = 1.7-2.7\%$

---

(13) Chevrel, R.; Sergent, M.; Meuri, J. L.; Quan, D. T.; Colin, Y. *J. Solid State Chem.* **1974**, *10*, 260.

(14) David, W. I. F.; Johnson, M. W.; Knowles, K. J.; Moreton-Smith, C. M.; Crosbie, G. D.; Campbell, E. P.; Graham, S. P.; Lyall, J. S. Rutherford Appleton Laboratory Report, RAL-86-102, 1986.

(15) Larson, A. C.; von Dreele, R. B. General Structure Analysis System; Report LAUR 86-748; Los Alamos Laboratory, Los Alamos, NM, 1994.

(16) De Jonge, R.; Poppma, T. J. A.; Wiegers, G. A.; Jellinek, F. *J. Solid State Chem.* **1970**, *2*, 188.

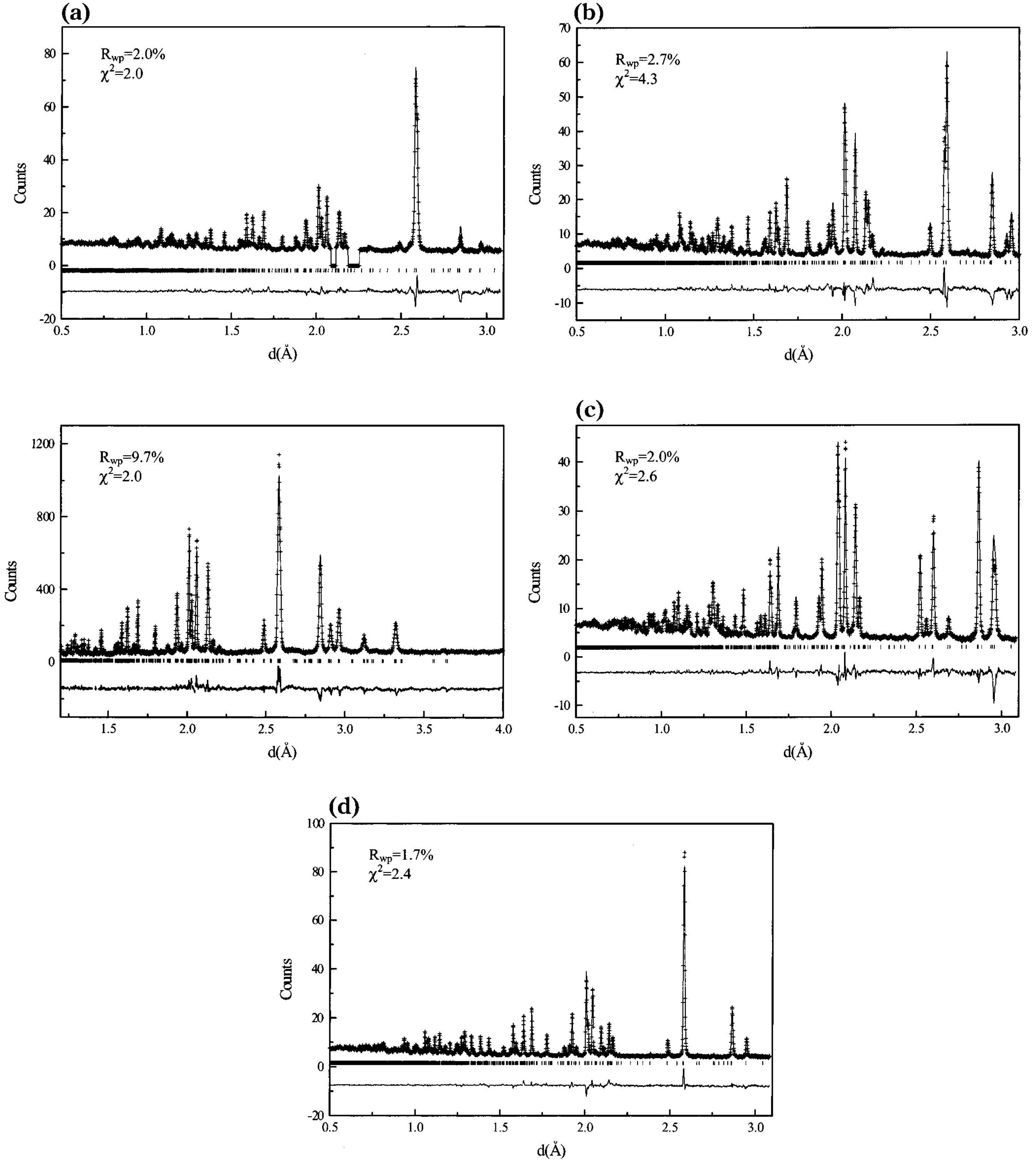

Figure 1. Observed (crosses), calculated (upper full line), and difference (lower full line) room temperature powder diffraction profiles of (a) VMo_2S_4 (neutron data: upper plot; X-ray data: lower plot), (b) $CrMo_2S_4$ (neutron data), (c) $FeMo_2S_4$ (neutron data), and (d) $CoMo_2S_4$ (neutron data). Data were collected in the backscattering detector banks. All refinements were carried out in the space group *Cc*. Reflection positions are marked.

in *Cc*; χ^2 = 3.3−10.0, R_{wp} = 2.8−3.4% in *C*2/*m*). To confirm that these improvements were not merely the result of an increase in the number of variables, refinements were also carried out in the space group *Cm* which produced similar quality refinements to those in *C*2/*m*, even with a larger number of variable parameters.

Final, observed, calculated, and difference profiles for refinements carried out in the space group *Cc* are given in Figure 1. The profiles for the short *d* spacing region for $CoMo_2S_4$, for refinements carried out in both space groups, are shown in Figure 2. There are clearly some mismatches in intensity and more pronounced features in the difference curve for the refinement in the space

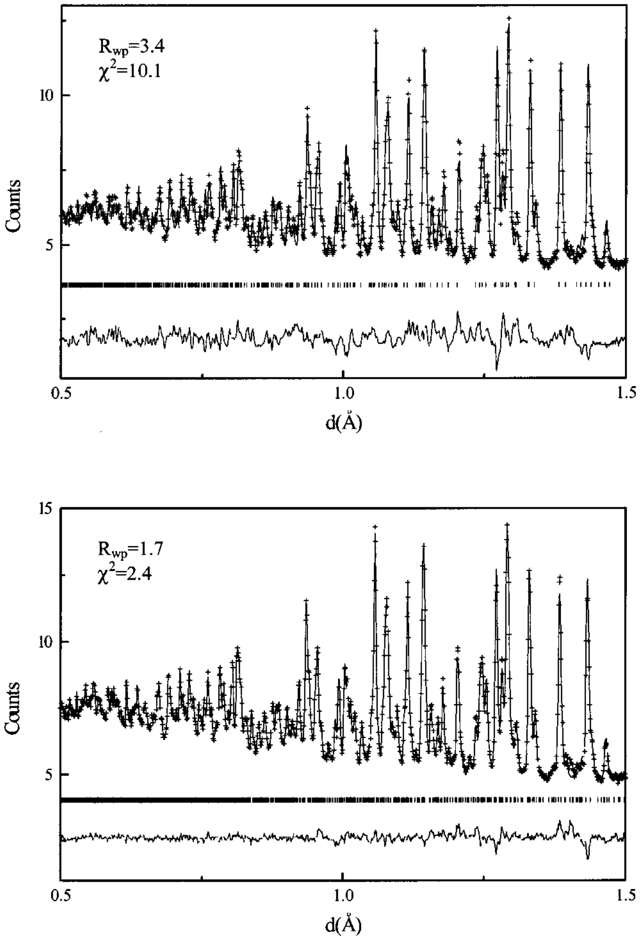

Figure 2. Comparison of the short *d* spacing region of the fitted room temperature neutron diffraction profiles for $CoMo_2S_4$ for refinements carried out in the *C*2/*m* space group (upper plot) and *Cc* space group (lower plot).

group *C*2/*m* than in *Cc*. The final refined parameters for the AMo_2S_4 materials, in the space group *Cc*, are presented in Table 2. Selected cation−cation and cation−anion distances are provided as Supporting Information.

Table 2. Refined Parameters for AMo_2S_4 (A = V, Cr, Fe, Co) at Room Temperature

		A			
		V	Cr	Fe	Co
a/Å		11.8747(2)	11.8431(3)	11.8148(2)	11.7966(2)
b/Å		6.4860(1)	6.4964(1)	6.5499(1)	6.5504(1)
c/Å		12.825(2)	12.8221(3)	13.014(2)	12.6950(2)
β		114.722(1)	113.949(2)	114.455(1)	115.530(1)
	B/Å^2 [a]	0.143(2)	0.25(1)	0.257(2)	0.31(1)
(A(1))	SOF A	0.876(3)	1.0	1.0	1.0
	SOF Mo	0.124(3)	0.0	0.0	0.0
	x	0.579(−)[b]	0.598(−)[b]	0.5872(−)[b]	0.585(−)[b]
	y	0.109(5)	0.108(1)	0.130(1)	0.117(2)
	z	−0.048(−)[b]	−0.043(−)[b]	−0.048(−)[b]	−0.040(−)[b]
(A(2))	SOF A	0.876(3)	1.0	1.0	1.0
	SOF Mo	0.124(3)	0.0	0.0	0.0
	x	0.562(4)	0.588(2)	0.5664(4)	0.574(1)
	y	0.346(4)	0.391(1)	0.3844(8)	0.373(3)
	z	0.440(4)	0.453(2)	0.4495(3)	0.454(1)
[B(1)]	SOF A	0.063(2)	0.0	0.0	0.0
	SOF Mo	0.937(2)	1.0	1.0	1.0
	x	0.733(3)	0.7382(9)	0.731(1)	0.7374(9)
	y	0.6023(5)	0.630(1)	0.601(1)	0.6029(9)
	z	0.193(3)	0.207(1)	0.205(1)	0.2124(6)
[B(2)]	SOF A	0.063(2)	0.0	0.0	0.0
	SOF Mo	0.937(2)	1.0	1.0	1.0
	x	0.431(4)	0.4264(9)	0.430(1)	0.4356(9)
	y	0.8703(8)	0.9014(6)	0.892(1)	0.8954(9)
	z	0.182(3)	0.1918(9)	0.196(1)	0.2017(6)
[B(3)]	SOF A	0.063(2)	0.0	0.0	0.0
	SOF Mo	0.937(2)	1.0	1.0	1.0
	x	0.425(4)	0.432(1)	0.4251(7)	0.426(1)
	y	0.3583(7)	0.3516(7)	0.348(1)	0.3514(8)
	z	0.181(3)	0.194(1)	0.1919(7)	0.1894(6)
[B(4)]	SOF A	0.063(2)	0.0	0.0	0.0
	SOF Mo	0.937(2)	1.0	1.0	1.0
	x	0.740(4)	0.7412(9)	0.7410(7)	0.742(1)
	y	0.1489(7)	0.121(1)	0.144(1)	0.1441(8)
	z	0.197(3)	0.2078(9)	0.2079(6)	0.2065(7)
S(1)	*x*	0.301(4)	0.302(1)	0.294(2)	0.293(1)
	y	0.121(2)	0.120(2)	0.120(3)	0.115(1)
	z	0.040(3)	0.056(1)	0.054(2)	0.0475(9)
S(2)	*x*	0.366(4)	0.365(2)	0.362(2)	0.368(1)
	y	0.867(2)	0.871(3)	0.882(3)	0.872(2)
	z	0.333(3)	0.344(2)	0.346(2)	0.3515(9)
S(3)	*x*	0.598(4)	0.590(1)	0.584(2)	0.587(1)
	y	0.628(2)	0.630(4)	0.620(3)	0.622(2)
	z	0.303(3)	0.310(2)	0.306(2)	0.3019(8)
S(4)	*x*	0.577(4)	0.573(2)	0.577(2)	0.579(1)
	y	0.876(2)	0.881(3)	0.879(4)	0.880(2)
	z	0.083(3)	0.088(2)	0.095(2)	0.0874(8)
S(5)	*x*	0.596(4)	0.599(2)	0.596(2)	0.599(1)
	y	0.129(2)	0.118(3)	0.125(3)	0.134(2)
	z	0.299(3)	0.314(2)	0.312(2)	0.315(1)
S(6)	*x*	0.565(4)	0.576(2)	0.564(2)	0.568(1)
	y	0.365(2)	0.371(4)	0.370(3)	0.370(2)
	z	0.074(3)	0.090(2)	0.088(2)	0.0821(9)
S(7)	*x*	0.314(4)	0.318(1)	0.312(2)	0.314(1)
	y	0.619(2)	0.625(3)	0.629(3)	0.635(1)
	z	0.048(3)	0.062(1)	0.064(2)	0.058(1)
S(8)	*x*	0.362(4)	0.362(1)	0.345(2)	0.358(1)
	y	0.365(2)	0.371(3)	0.370(3)	0.377(2)
	z	0.330(3)	0.346(2)	0.336(2)	0.340(1)
R_{wp}/%		2.0 9.7	2.7	2.0	1.7
χ^2		2.0	4.3	2.6	2.4

[a] Thermal parameters of all atoms were constrained to be equal.
[b] Fixed to define the origin.

Transport Properties. Plots of resistivity vs temperature exhibit negative slopes, consistent with semiconducting behavior (Figure 3a). The materials with A = V, Cr show a weaker temperature dependence than those containing Fe and Co. Furthermore, for all phases the temperature dependence of the resistivity does not follow an Arrhenius law. However, plots of ln(ρ) vs $T^{-1/4}$ are linear over a wide temperature range, consistent with a variable range hopping conduction mechanism (Figure 3b).

Magnetic Properties. Magnetic susceptibility curves for the AMo_2S_4 phases are presented in Figure 4. The material VMo_2S_4 exhibits paramagnetic behavior down to the lowest temperature studied. Data over the temperature range 15−320 K can be described by a modified Curie−Weiss law, $\chi = \chi_0 + C/(T - \theta)$, incorporating a temperature-independent term. Derived parameters are presented in Table 3. If the magnetic moment is associated exclusively with the vanadium cations, the Curie constant, $C = 0.1035(8)$, leads to an estimated effective magnetic moment of $\mu_{eff} = 0.91(1)\mu_B$ per vanadium ion, which is considerably smaller than the spin-only value for V^{2+} or V^{3+}. $CrMo_2S_4$ is also paramagnetic, although there is a weak feature in the magnetic susceptibility at 25 K. However, low-temperature neutron diffraction measurements indicate the absence of long-range magnetic ordering down to 1.4 K.[17] Data above 80 K can be described by a modified Curie−Weiss law (Table 3). The effective moment as-

---

(17) D'Anterroches Meneau, C.; Boucher, B. *Acta Crystallogr.* **1977**, *B33*, 1495.

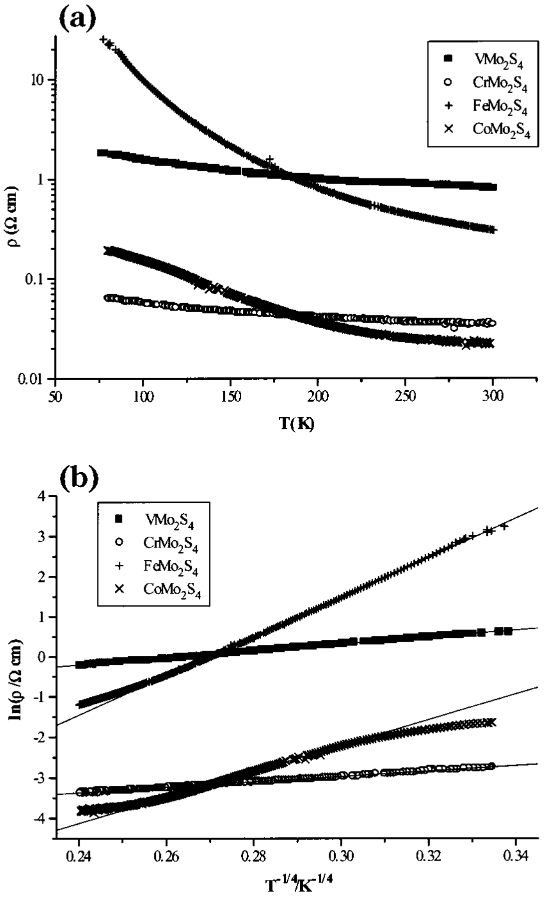

Figure 3. (a) Temperature dependence of the electrical resistivity of AMo_2S_4 phases and (b) $T^{-1/4}$ dependence of $\ln(\rho)$; the solid line shows the best linear fit.

Table 3. Parameters Derived from Magnetic Susceptibility Data with a Modified Curie−Weiss Law

material	data range/K	χ_0/emu	C/emu·K^{-1}	θ/K	μ_{exp}(A)
VMo_2S_4	15−320	$6.50(7) \times 10^{-4}$	0.1035(8)	−0.6(1)	0.91(1)
$CrMo_2S_4$	80−320	$1.75(6) \times 10^{-3}$	0.67(3)	−64(4)	2.3(1)
$FeMo_2S_4$	200−320		3.94(6)	−347(1)	5.61(9)

sociated with the chromium cations is 2.3(1)μ_B, which is considerably lower than the spin-only value for either Cr^{2+} or Cr^{3+}, and the Weiss constant is −64(4) K, indicating the presence of antiferromagnetic interactions. The moderately high value of the temperature-independent contribution to the magnetic susceptibility of VMo_2S_4 and $CrMo_2S_4$ suggests some degree of electron delocalization, which would be consistent with the relatively low values of resistivity exhibited by these materials. The magnetic susceptibility of $FeMo_2S_4$ shows a weak temperature dependence, with a broad maximum at 150 K. This is a characteristic feature of low-dimensional magnetic behavior.[18] The magnetic ordering temperature, determined from the maximum in $d\chi/dT$, is 105(5) K, close to the value of 110 K reported in a variable temperature neutron powder diffraction study.[17] The abnormal temperature dependence of the susceptibility above the ordering temperature may be explained by the retention of two-dimensional ordering of iron cations within the *ab* planes, despite the disappearance of three-dimensional magnetic order at T_N. Above 200 K, the susceptibility data follow a Curie−Weiss law. The effective magnetic moment of the iron cations is 5.61(9) μ_B. The deviation of this value from the spin-only magnetic moment of 5.92 μ_B predicted for high-spin Fe^{3+} is considerably greater than could be accounted for by an orbital contribution to the ^6A ground state of a hs-d^5 ion. The value is comparable to that expected for high-spin Fe^{2+} ions with spin−orbit coupling and is similar to that obtained previously, from data collected over a wider range of temperatures and attributed to high-spin Fe^{2+}.[13] The magnetic susceptibility of $CoMo_2S_4$ exhibits weak temperature dependence, with a broad minimum at 60 K and does not follow a Curie−Weiss law at any temperature in the range $5 \leq T/K \leq 320$. The general form of the curve is similar to that of $FeMo_2S_4$ below 150 K. It has been suggested on the basis of high-temperature magnetic susceptibility data that $CoMo_2S_4$ orders antiferromagnetically at 350 K.[10] Low-temperature powder neutron diffraction data reported here show intense magnetic Bragg peaks at long *d* spacings. These peaks are absent from the neutron diffraction data collected at 300 K and recent variable temperature measurements indicate that three-dimensional long-range magnetic order is only established below ca. 120 K. Details of the magnetic structure refinement are presented below.

Low-Temperature Powder Neutron Diffraction Data. At low temperatures, a number of additional reflections are apparent at long *d* spacings in the neutron diffraction data collected for $FeMo_2S_4$ and $CoMo_2S_4$. All of these reflections can be indexed using the crystallographic unit cell. Therefore, the magnetic unit cell is identical in size with the crystallographic unit cell and the propagation vector is (0,0,0). The crystallographic structure determined at room temperature was used for the initial structural model at 4 K. The atomic parameters were established with Rietveld refinements using neutron diffraction data from the backscattering bank of detectors. Simultaneous refinements using data collected in the low-angle bank of detectors and in the backscattering bank of detectors were carried out to determine the magnetic structures. The magnetic structure determined by D'Anterroches Meneau et al.[17] for $FeMo_2S_4$ was used as a starting model. The free-ion form factors[19] for Fe^{2+} and Co^{2+} were used to describe the angular dependence of the magnetic scattering. Background terms, peak shape parameters, lattice parameters, and an overall thermal parameter were refined. Data for both $FeMo_2S_4$ and $CoMo_2S_4$ can be successfully described with localized moments associated with the A cations only. The *y* component of the moment associated with the A cations refined to values close to zero, the value at which it was subsequently fixed. The *x* and *z* components of the A-site moments were refined, and their final values, together with other final refined parameters, are presented in Table 4. Final observed, calculated, and difference profiles are given in Figure 5.

Discussion

Refinements using neutron diffraction data have established that the AMo_2S_4 phases exhibit a structure

---

(18) de Jongh, L. J.; Miedema, A. R. *Adv. Phys.* **1974**, *23*, 1.

(19) Brown, P. J. In *International Tables for Crystallography*; Wilson, A. J. C., Ed.; Kluwer: Dordrecht, 1992; Vol. C, Chapter 4.

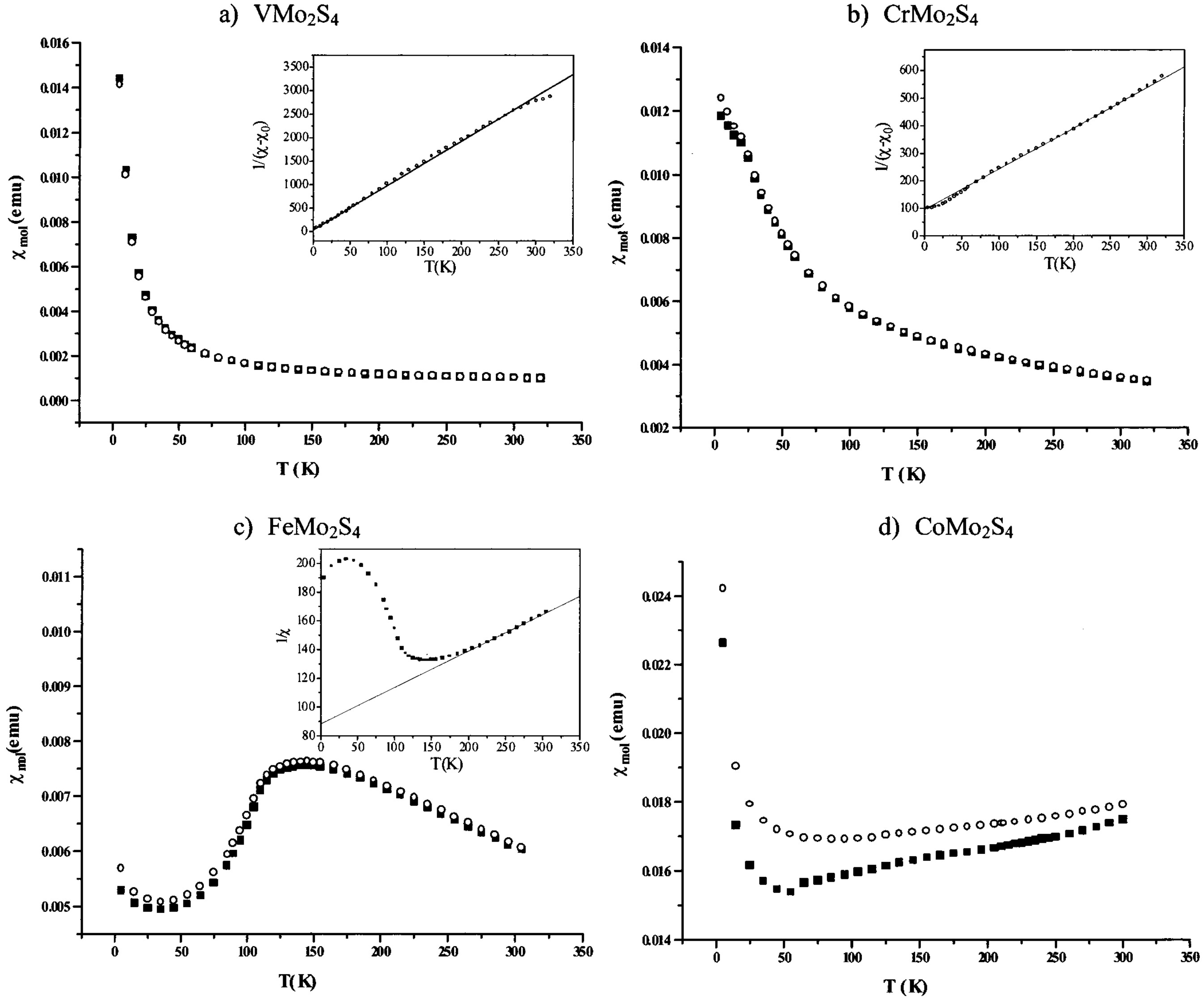

Figure 4. Zero-field-cooled (solid squares) and field-cooled (open circles) molar magnetic susceptibility data for (a) VMo_2S_4, (b) $CrMo_2S_4$, (c) $FeMo_2S_4$, and (d) $CoMo_2S_4$. The insets show the fit (solid line) to the modified Curie–Weiss expression for VMo_2S_4 and $CrMo_2S_4$ and Curie–Weiss expression for $FeMo_2S_4$.

similar to that of Cr_3S_4. The cation distribution established from the room-temperature data is of the normal type for A = Cr, Fe, and Co. However, in VMo_2S_4 12% of the V atoms resides in the fully occupied layer, and therefore the composition may be better expressed as $(V_{0.88}Mo_{0.12})[V_{0.12}Mo_{1.87}]S_4$. This behavior is markedly different from that of the AV_2S_4 materials (A = Ti, Cr, Fe, Ni), where the cation distribution changes progressively from an inverse to a normal type as the atomic number of A increases. This suggests that cations from the second transition series have a greater preference for sites in the fully occupied layer than do those from the first transition series and is consistent with our previous conclusions concerning the correlation between the cation distribution and the electronic properties of the constituent cations.[5–7]

In the ideal Cr_3S_4 structure, each cation in the fully occupied layer is surrounded by six neighbors, in a hexagonal array (Figure 6a). In the AMo_2S_4 phases, this ideal arrangement is distorted, with the cations in the fully occupied (MoS_2) layer being displaced from their ideal positions at the center of the octahedra. For a structure described in the space group *C*2/*m*, the only symmetry allowed distortion is the formation of zigzag chains directed along [010] within the MS_2 layers (Figure 6b). Tight-binding band structure calculations[8] carried out for MS_2 units exhibiting a zigzag distortion indicate that, for Mo(III):d^3, there would be a half-filled t_{2g}-derived conduction band. Hence, metallic behavior would be predicted, in contrast with the observed electrical transport properties. However, the significantly better agreement of the refinements carried out using the space group *Cc* suggests that this is the correct choice to describe these structures. This is corroborated by the absence of a center of symmetry in $FeMo_2S_4$, as reported by Guillevic et al.[12] Refinements carried out in space group *Cc* reveal metal clustering in which intercation distances are sufficiently short (<3 Å) to permit a high degree of cation–cation interaction. In $FeMo_2S_4$ and $CoMo_2S_4$, the cations in the fully occupied layer form clusters of four atoms, with a diamond shape, similar to that identified by Guillevic et al.[12] (Figure 7a). Band structure calculations carried out for MX_2 layers containing d^3 cations, such as Mo^{3+}, indicate that

Table 4. Refined Parameters for FeMo$_2$S$_4$ and CoMo$_2$S$_4$ at 4 K

		A	
		Fe	Co
a/Å		11.8036(5)	11.7987(2)
b/Å		6.5452(3)	6.5539(1)
c/Å		12.9757(6)	12.6863(3)
β		114.482(2)	115.612(2)
	B/Å$^{2\,a}$	0.29(1)	0.20(2)
(A(1))	x	0.5872(−)^b	0.5943(−)^b
	y	0.125(1)	0.129(2)
	z	−0.0475(−)^b	−0.0396(−)^b
	M$_x$	0.3(1)	0.3(1)
	M$_y$	0.0	0.0
	M$_z$	3.15(3)	2.12(4)
	moment/μ_B	3.16(3)	2.14(3)
(A(2))	x	0.5572(4)	0.5650(8)
	y	0.3852(9)	0.383(3)
	z	0.4546(5)	0.459(1)
	M$_x$	0.3(1)	0.3(1)
	M$_y$	0.0	0.0
	M$_z$	3.15(3)	2.12(4)
	moment/μ_B	3.16(3)	2.14(3)
[B(1)]	x	0.7201(8)	0.737(1)
	y	0.5729(9)	0.6098(9)
	z	0.1995(8)	0.2272(9)
[B(2)]	x	0.4155(8)	0.431(1)
	y	0.886(1)	0.9076(7)
	z	0.1923(9)	0.2286(9)
[B(3)]	x	0.414(1)	0.422(1)
	y	0.379(1)	0.3615(9)
	z	0.1992(9)	0.1991(9)
[B(4)]	x	0.726(1)	0.731(1)
	y	0.127(3)	0.1525(7)
	z	0.212(1)	0.2231(9)
S(1)	x	0.290(2)	0.299(2)
	y	0.119(3)	0.115(2)
	z	0.059(2)	0.077(1)
S(2)	x	0.356(2)	0.374(1)
	y	0.882(4)	0.887(2)
	z	0.347(2)	0.383(1)
S(3)	x	0.573(1)	0.577(1)
	y	0.612(3)	0.630(2)
	z	0.312(2)	0.315(1)
S(4)	x	0.558(2)	0.571(2)
	y	0.874(4)	0.887(2)
	z	0.091(2)	0.103(1)
S(5)	x	0.579(2)	0.600(1)
	y	0.111(2)	0.123(3)
	z	0.299(1)	0.332(1)
S(6)	x	0.560(2)	0.572(1)
	y	0.378(3)	0.360(2)
	z	0.082(1)	0.099(1)
S(7)	x	0.311(2)	0.307(2)
	y	0.638(4)	0.632(2)
	z	0.071(1)	0.084(1)
S(8)	x	0.338(2)	0.344(1)
	y	0.360(3)	0.378(2)
	z	0.344(2)	0.358(1)
R_{wp} 145° bank/%		5.44	4.50
R_{wp} 35° bank/%		6.02	6.02
χ^2		2.2	2.6

[a] Thermal parameters of all atoms were constrained to be equal. [b] Fixed to define the origin.

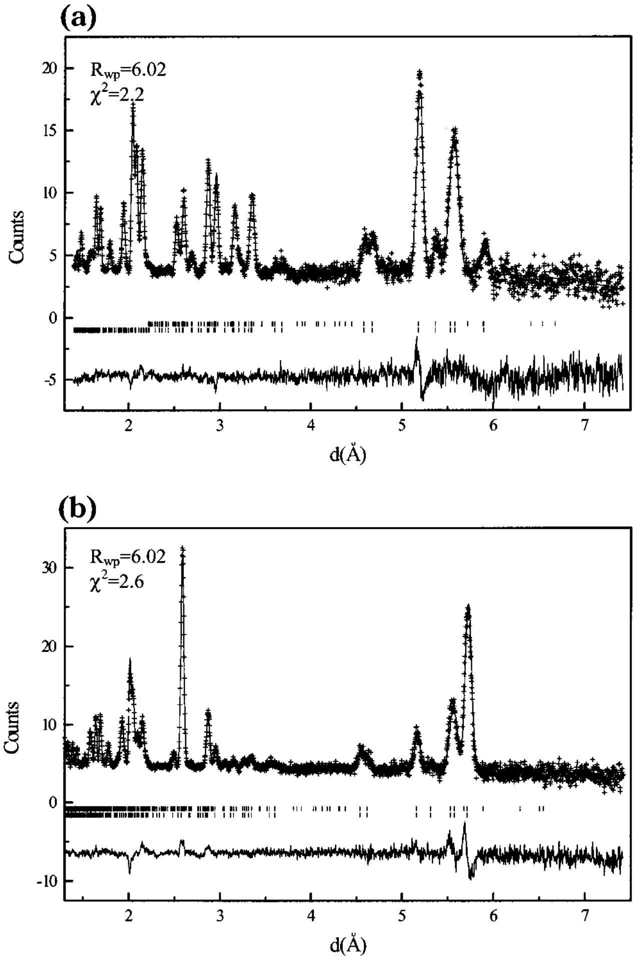

Figure 5. Final observed (crosses), calculated (upper full line), and difference (lower full line) neutron diffraction profiles for (a) FeMo$_2$S$_4$ and (b) CoMo$_2$S$_4$ at 4.2 K. Data were collected using the low-angle detector banks. Reflection positions are marked: the lower markers refer to the crystallographic unit cell (*Cc*) and the upper markers the magnetic unit cell described in the primitive space group *P*1.

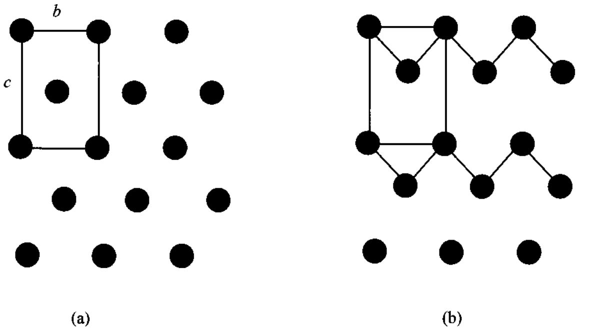

Figure 6. (a) Ideal hexagonal arrangement of cations in a dichalcogenide layer of edge-sharing MS$_6$ octahedra and (b) symmetry-allowed intralayer distortion involving the formation of zigzag chains of cations for a structure crystallizing in the space group *C*2/*m*.

the diamond-type clustering is a consequence of a Peierls distortion associated with half-filled t_{2g} block bands.[8] This results in the opening of a gap at the Fermi surface, accounting for the observed semiconducting behavior. The distortion in CrMo$_2$S$_4$ and VMo$_2$S$_4$ appears to be intermediate between zigzag chains and diamond clusters and involves the formation of chains containing triangular clusters. Although no band structure calculations have been carried out for this clustering scheme, the observed semiconducting properties suggest that the distortion results in a filled t_{2g}-derived band. A further difference between the AMo$_2$S$_4$ phases containing the early transition series cations V and Cr and those containing the later elements Fe and Co is observed in the structure of the vacancy layer. In this layer, the A cations form chains directed along [010]. The intrachain cation−cation separation in AMo$_2$S$_4$ with A = Fe, Co is ca. 3.3 Å whereas in the materials

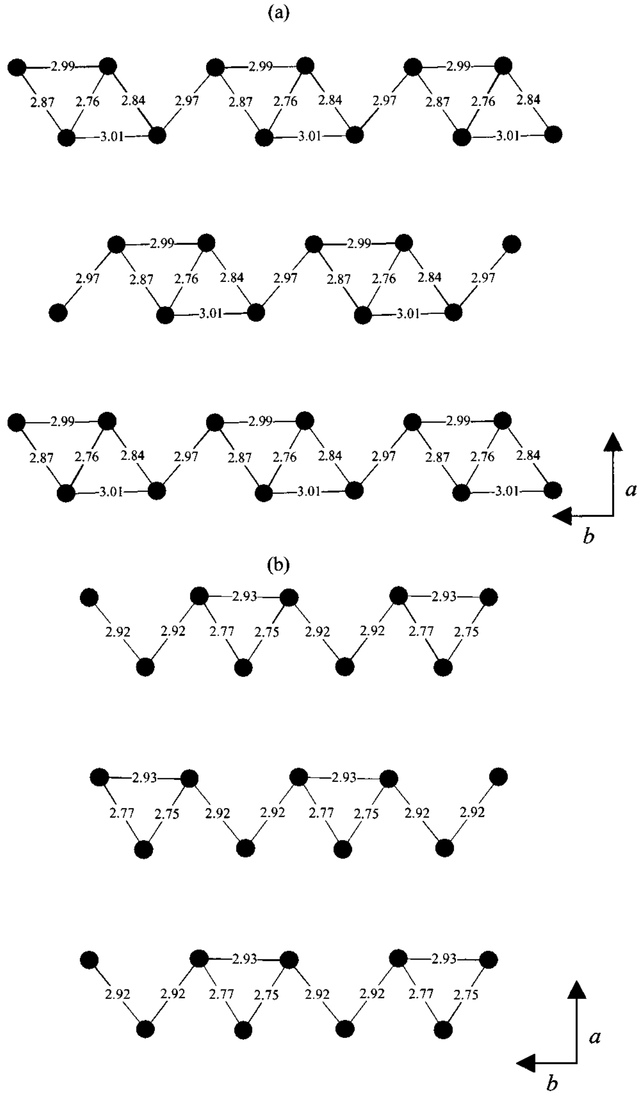

Figure 7. Arrangement of cations in the fully occupied layer of AMo_2S_4 phases determined by powder neutron diffraction. (a) Distortion scheme involving the formation of diamond-type clusters in $CoMo_2S_4$. (b) Distortion scheme involving the formation of triangular clusters of cations in $CrMo_2S_4$. $FeMo_2S_4$ and VMo_2S_4 exhibit distortions corresponding to schemes (a) and (b), respectively. Solid lines indicate short cation−cation separations at the distances marked.

containing vanadium and chromium there is an alternation of short (2.96 Å) and long (3.54 Å) cation−cation distances along the chain.

The structure of the AMo_2S_4 materials exhibit similarities with those of A_xTaS_2 and A_xNbS_2 (A = V, Cr, Mn, Fe, Co, and Ni; x = 1/4 and 1/3)[20−22] in which the first-row transition metals are intercalated between the layers of the dichalcogenides TaS_2 and NbS_2. The A_xTaS_2 and A_xNbS_2 phases are metallic and order magnetically at low temperatures, but only the 3d ions exhibit localized moments, while electrons in the MS_2 layers are delocalized.[23] When A is drawn from the early part of the transition series, RKKY interactions are dominant, giving rise to ferromagnetic behavior, while in the second half of the transition series superexchange interactions become progressively larger, leading to predominantly antiferromagnetic couplings. In AMo_2S_4, RKKY interactions are absent, owing to the nonmetallic nature of the materials, and for the early transition series cations A = V, Cr, the superexchange interactions are too weak to produce long-range magnetic ordering. However, the increase in the strength of the superexchange interactions on moving to the later transition series cations A = Fe, Co is sufficient to lead to long-range magnetic ordering.

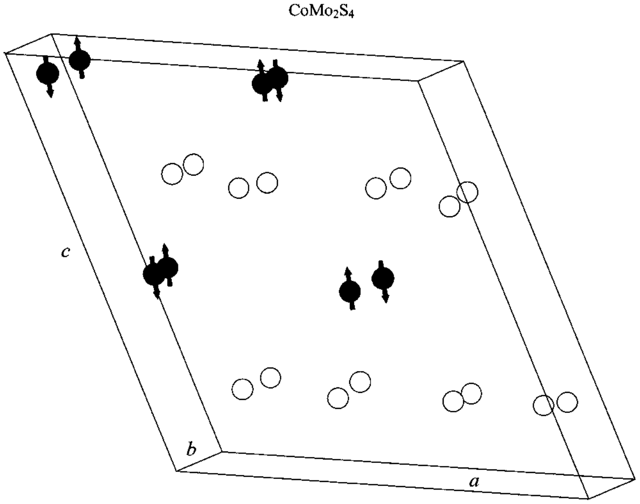

Figure 8. Magnetic structure of $CoMo_2S_4$ at 4.2 K. Sulfide anions are omitted for clarity. Open circles represent molybdenum cations in the fully occupied layer and solid circles represent cobalt cations in the vacancy layer. The crystallographic unit cell, which is marked, is coincident with the magnetic unit cell.

$FeMo_2S_4$ and $CoMo_2S_4$ exhibit a similar magnetic structure, with localized moments associated with the A cations only (Figure 8). The moments are reduced from the spin-only values for Fe^{2+} and Co^{2+}. The reduction of 20% for Fe and 27% for Co is comparable with that observed in related materials[24−26] and may be attributed to the transfer of spin from the cation, owing to the covalency of the A−S interaction. These moments are oriented almost perpendicular to the cation layers. In each vacancy layer, the moment on a given A cation is antiparallel with those of its four nearest neighbors and parallel with moments of its four next-nearest neighbors. Using the values of the Néel temperature and the Weiss constant, D'Anterroches Meneau et al.[17] estimated the magnitude of the nearest neighbor magnetic exchange interactions in $FeMo_2S_4$ and concluded that all are negative but the interactions within the layers are much stronger than those between layers.

The magnetic structure of $FeMo_2S_4$ and $CoMo_2S_4$ determined here differs from that of the structurally related phases $NiCr_2S_4$[24,25] and FeV_2S_4,[4] whose mag-

---

(20) Friend, R. H.; Beal, A. R.; Yoffe, A. D. *Philos. Mag.* **1977**, *35*, 1269.

(21) Anzenhofer, K.; van der Berg, J. M.; Cossee, P.; Helle, J. N. *J. Phys. Chem. Solids* **1970**, *31*, 1057.

(22) van Laar, B.; Rietveld, H. M.; Ijdo, D. J. W. *J. Solid State Chem.* **1971**, *3*, 154.

(23) Parkin, S. S. P.; Friend, R. H. *Philos. Mag. B* **1980**, *41*, 65.

(24) Powell, A. V.; Colgan, D. C.; Ritter, C. *J. Solid State Chem.* **1997**, *134*, 110.

(25) Powell, A. V.; Colgan, D. C.; Ritter, C. *J. Solid State Chem.* **1999**, *143*, 163.

(26) Hamasaki, T.; Hashimoto, T.; Yamaguchi, Y.; Watanabe, H. *Solid State Commun.* **1975**, *16*, 895.

netic structures involve localized moments in both the vacancy and fully occupied layers and are described by propagation vectors ($^1/_2$,0,$-^1/_2$) and ($^1/_2$,0,$^1/_2$), respectively. This gives rise to sheets of ferromagnetically coupled ions, inclined at an angle of ca. 45° with the MS_2 layers. Neighboring sheets are coupled antiferromagnetically with respect to each other. The magnetic structure of AMo_2S_4 (A = Fe, Co) involves localized moments of the A cations only. However, the different arrangement of the vacancy layer moments, a consequence of the (0,0,0) propagation vector, does not result in ferromagnetically coupled sheets of ions. The magnetic structure may instead be considered in terms of chains of antiferromagnetically coupled cations directed along [010]. Neighboring chains in the *ab* plane, which are separated by ca. 5.5 Å, are antiferromagnetically aligned.

In conclusion, we have established that the correct choice of space group for the description of the structure of the AMo_2S_4 phases is *Cc*, which is compatible with the observed electron transport properties. All four phases exhibit a distortion of the metal dichalcogenide unit, the extent of which varies with the position of the A cation in the transition series. For the early series elements A = V, Cr, we have identified a novel triangular clustering scheme whereas materials containing the later elements Fe and Co exhibit a diamond-type distortion. The A cation also has a marked influence on the magnetic properties. The increasing strength of the superexchange interaction across the first transition series leads to long-range magnetic order in materials containing the later transition series cations. Low-temperature neutron diffraction has provided the first confirmation of magnetic order in $CoMo_2S_4$ and demonstrates that the magnetic structure is identical to that of $FeMo_2S_4$.

Acknowledgment. We thank the EPSRC for a grant in support of our neutron scattering program, The Leverhulme Trust for a research fellowship for P.V., Heriot-Watt University for a research scholarship for M.L.K., and Dr R.I. Smith (Rutherford Appleton Laboratory) for assistance with the collection of neutron diffraction data.

Supporting Information Available: Tables of metal−metal distances and cation−anion distances (PDF). This material is available free of charge via the Internet at http://pubs.acs.org.

CM010720K